https://doi.org/10.5194/egusphere-2024-1163
Preprint. Discussion started: 25 June 2024

Unheralded contributions of biogenic volatile organic compounds from urban greening to ozone pollution: a high-resolution modeling study

Haofan Wang[1,2,3,4], Yuejin Li[1,2,3], Yiming Liu[1,2,3]*, Xiao Lu[1,2,3], Yang Zhang[5], Qi Fan[1,2,3]*, Tianhang Zhang[4], Chong Shen[6]

[1]*School of Atmospheric Sciences, Sun Yat-sen University, and Southern Marine Science and Engineering Guangdong Laboratory (Zhuhai), Zhuhai, 519082, PR China*
[2]*Guangdong Provincial Field Observation and Research Station for Climate Environment and Air Quality Change in the Pearl River Estuary, Guangzhou, 510275, PR China*
[3]*Guangdong Province Key Laboratory for Climate Change and Natural Disaster Studies, Sun Yat-sen University, Zhuhai, PR China*
[4]*Centre for Atmospheric Science, Department of Earth and Environmental Sciences, University of Manchester, Manchester, United Kingdom*
[5]*College of Resources and Environment, Chengdu University of Information Technology, Chengdu, Sichuan, China*
[6]*Guangzhou Climate and Agrometeorology Center, Guangzhou 511430, China*

Correspondence to: Yiming Liu (liuym88@mail.sysu.edu.cn), Qi Fan (eesfq@mail.sysu.edu.cn)

https://doi.org/10.5194/egusphere-2024-1163
Preprint. Discussion started: 25 June 2024

Abstract

Urban Green Spaces (UGS) are widely advocated for mitigating urban atmospheric environment. However, this study reveals that it can exacerbate urban ozone (O_3) levels under certain conditions, as demonstrated by a September 2017 study in Guangzhou, China. Utilizing the Weather Research and Forecasting Model with the Model of Emissions of Gases and Aerosols from Nature (WRF-MEGAN) and the Community Multiscale Air Quality (CMAQ) model with a high horizontal resolution (1 km), we assessed the impact of UGS-related biogenic volatile organic compound (BVOC) emissions on urban O_3. Our findings indicate that UGS-BVOC emissions in Guangzhou amounted to 666.49 Gg, primarily from isoprene (ISOP) and terpenes (TERP). These emissions contribute ~30% of urban ISOP concentrations and their incorporations to the model significantly reduce the underestimation against observations. The study shows improvements in simulation biases for NO_2, from 7.01 μg/m^3 to 6.03 μg/m^3, and for O_3, from 7.77 μg/m^3 to -1.60 μg/m^3. UGS-BVOC and UGS-LUCC (land use cover changes) integration in air quality models notably enhances surface monthly mean O_3 predictions by 3.6-8.0 μg/m^3 (+3.8-8.5%) and contributes up to 18.7 μg/m^3 (+10.0%) to MDA8 O_3 during O_3 pollution episodes. Additionally, UGS-BVOC emissions alone increase the monthly mean O_3 levels by 2.2-3.0 μg/m^3 (+2.3-3.2%) in urban areas and contribute up to 6.3 μg/m^3 (+3.3%) to MDA8 O_3 levels during O_3 pollution episodes. These impacts can extend to surrounding suburban and rural areas through regional transport, highlighting the need for selecting low-emission vegetation and refining vegetation classification in urban planning.

Keywords

Urban green space; BVOC; Ozone; Land use cover; CMAQ; MEGAN

1. Introduction

Exposure to air pollution now accounts for more fatalities than malaria, tuberculosis, and HIV/AIDS combined (Lelieveld et al., 2020). As a result, the World Health Organization has declared air pollution the most significant environmental threat to human health (WHO, 2021). Notably, over 70% global health burden of air pollution stems from human-made emissions, leading to a policy focus predominantly on reducing these

https://doi.org/10.5194/egusphere-2024-1163
Preprint. Discussion started: 25 June 2024

emissions (Chowdhury et al., 2022; Lelieveld et al., 2019). Despite proactive measures to curb anthropogenic emissions, the incidence of ozone episodes is escalating alongside rapid urbanization (Lu et al., 2020; Yim et al., 2019). Numerous studies have investigated the effects of land use cover changes (LUCC) on air quality during urbanization using numerical models and the majority of these studies conclude that urbanization exacerbates air pollution (Qiu et al., 2023; Wang et al., 2022). However, such studies that depend on numerical models usually face the coarse-resolution land use cover data limitation (Ma et al., 2022, 2019), which leads these studies to frequently overlook a passive abatement approach distinct from reducing anthropogenic sources—namely, the cultivation of urban green spaces (UGS) (Cohen et al., 2017).

The widely accepted notion that UGS can enhance air quality is substantiated by various strands of literature, including public health (Burnett et al., 2018), urban planning (Solomon, 2007), and ecosystem services (Lohmann et al., 2010). This concept is not only prevalent in scholarly circles but also gains traction in popular media and is echoed in international standards and policy frameworks. For instance, the United Nations System of Environmental-Economic Accounting advocates for vegetation as a nature-based approach to mitigate air pollution (Le Page et al., 2015). Vegetation primarily contributes to air pollution reduction through two mechanisms: deposition and dispersion (Shindell et al., 2012). Deposition involves the absorption of air pollutants onto vegetative surfaces, while dispersion refers to the reduction of air pollutant concentrations through aerodynamic effects caused by vegetation (Zhao et al., 2022). Notably, dispersion effects are significantly more impactful than deposition, exceeding it by an order of magnitude (Ramanathan et al., 2001).

However, the efficacy of dispersion effects resulting from UGS-LUCC in reducing air pollution is not straightforward. These effects can, under certain conditions, even increase local air pollution concentrations. These conditions are influenced by several factors, such as the specific structure of the UGS vegetation properties (e.g., height, leaf density), the site context (e.g., street canyon geometry, proximity to emission sources), and prevailing meteorological conditions (e.g., wind speed and direction) (Ramanathan et al., 2001; Solomon, 2007). For example, dense tree canopies might impede ventilation in urban street canyons, while porous vegetation barriers in open-road settings could potentially intensify roadside air pollution concentrations (Allen and Ingram, 2002; Cohen et al., 2017). Furthermore, Seinfeld et al., (1998) underscores the complexity of these interactions, and they demonstrated that vegetation could exert nonlinear effects on meteorological processes. These effects are particularly evident in their impact on the Planetary Boundary Layer Height (PBLH) and the turbulent transport and advection of pollutants, which in turn influence dispersion conditions.

https://doi.org/10.5194/egusphere-2024-1163
Preprint. Discussion started: 25 June 2024

UGS also have a complex role in air quality due to their production of biogenic volatile organic compounds (BVOCs). For instance, in cities like Los Angeles, the UGS-BVOC emissions contribute to a quarter of the secondary organic aerosol formation on hot days (Ramanathan et al., 2005). While Guenther et al., (2012) noted that the majority of BVOC emissions are from natural land cover, Ma et al., (2022) indicates that in metropolitan areas, the UGS-BVOC emissions can be significantly higher, ranging from 1 to 30 times those from natural land use cover. This evidence suggests a dual nature of UGS vegetation in urban environments: it can mitigate air pollution under certain conditions, but conversely, there is substantial experimental and modelling evidence showing it can exacerbate pollution under different circumstances (Allen and Ingram, 2002; Burnett et al., 2018; Cohen et al., 2017). Moreover, metropolitan areas often encounter VOC-limited conditions, or NO_x-saturation, where even minimal BVOC emissions can lead to notable O_3 production (Wang et al., 2019). Additionally, urban areas typically experience higher temperatures than their surrounding natural landscapes due to the urban heat island effect (Masson-Delmotte et al., 2021). This increase in temperature is likely to further amplify the UGS-BVOC emissions (Zhou et al., 2015), influencing O_3 concentrations significantly. This interaction might explain why many regional numerical models underestimate urban surface ozone levels, as they often lack high-resolution land use cover data necessary to accurately estimate the UGS-BVOC emissions (Qiu et al., 2023; Wang et al., 2021; Wu et al., 2020).

Currently, there is a growing research interest in characterizing the air quality impacts of UGS. While Arghavani et al., (2019) investigating the effects of UGS on gaseous air pollutants in Tehran using the WRF-Chem model, their focus was on the impact of meteorological changes on O_3 resulting from UGS (i.e., UGS-LUCC effects), rather than the UGS-BVOC emissions effects on O_3. In contrast, Schlaerth et al., (2023a) addressed the influence of the UGS-BVOC emissions on O_3 in Los Angeles and their findings indicate that the UGS-BVOC emissions may increase O_3 by 0.95 ppb during the daytime and decrease it by 0.41 ppb at night. Despite Schlaerth et al., (2023a) illustrating the significance of the UGS-BVOC emissions on O_3 concentrations, they did not investigate the impact of the UGS-LUCC effects.

The nonlinear correlation between O_3 and concentrations of BVOC and NO_x underscores the importance of examining potential interactions between the UGS-BVOC emissions and anthropogenic emissions. Furthermore, recent studies have highlighted the significance of the UGS-LUCC effects and the UGS-BVOC emissions effects. Given the rise in urban O_3 pollution, investigating the influence of the UGS-LUCC effects and the UGS-BVOC emissions effects on O_3 can assist in rationalizing UGS planning and formulating air

https://doi.org/10.5194/egusphere-2024-1163
Preprint. Discussion started: 25 June 2024

quality mitigation strategies. However, there is a lack of quantification regarding the combined effects of UGS-LUCC and UGS-BVOC emissions on O_3.

Situated in South China, Guangzhou is one of the rapidly expanding cities in China since the initiation of the reform and opening-up policy, undergoing swift urbanization (Yao and Huang, 2023). Being a key city in the Guangdong-Hongkong-Macao Greater Bay Area, Guangzhou places significant emphasis on UGS development. In this study, we aim to reconstruct the leaf area index (LAI) dataset for urban areas and estimate the UGS-BVOC emissions utilizing the Model of Emissions of Gases and Aerosols from Nature version 3.1 (MEGANv3.1) (Guenther et al., 2020a). Subsequently, employing the Weather Research and Forecast model version 4.1.1 (WRFv4.1.1) (Salamanca et al., 2011) – Community Multiscale Air Quality model version 5.4 (CMAQv5.4) (https://zenodo.org/record/7218076, last accessed: June 3, 2023), we intend to estimate the improvements of the CMAQ simulation performance from considering UGS-LUCC and UGS-BVOC and investigate the UGS-LUCC effects, the UGS-BVOC emissions effects, and their combined impacts on O_3 over Guangzhou by configuring sensitivity scenarios.

2. Methods and data

2.1 Leaf area index and land cover dataset

The default LAI dataset to drive the MEGANv3.1 model is derived from the enhanced Moderate Resolution Imaging Spectroradiometer (MODIS) /MOD15A2H in 2003 with 1 km spatial resolution (Myneni et al., 2015). As MODIS/MOD15A2H assigns an LAI value of 0 to urban areas, MEGANv3.1 compensates by averaging the LAI values in the vicinity of the urban area. However, this approach introduces considerable uncertainty in the estimation of UGS-BVOC emissions. Hence, we opted for the Global Land Surface Satellite (GLASS) LAI product for MEGANv3.1 in 2017 with 500-m spatial resolutions, derived from MODIS surface reflectance data using the bidirectional long short-term memory (Bi-LSTM) model, which leverages existing global LAI products (Ma and Liang, 2022) and effectively incorporates the temporal and spectral information of MODIS surface reflectance. Consequently, the valid values of this data extend to urban areas, making it suitable for simulating the UGS-BVOC emissions.

In this study, UGS are delineated as vegetation areas within the urban grid, and the urban grids are derived from MODIS/MCD12Q1 (Friedl and Sulla-Menashe, 2019) in 2017, which corresponds to the simulation period with 500 m spatial resolution. Furthermore, a high-resolution (10 m) land cover dataset in 2017 was also obtained from the Geographic Remote Sensing Ecological Network Platform (accessible at http://www.gisrs.cn/infofordata?id=1c089287-909e-4394-b07f-c7004be60884, last accessed: 20/11/2023) and was employed to depict the spatial patterns of UGS. The processed land cover dataset is illustrated in Figure S1. Meanwhile, the use of high-resolution land use cover data is pivotal for accurately depicting the intricate details of land use cover, especially in areas broadly classified as urban by coarse-resolution data (i.e., MCD12Q1) and this refined approach allows for a more precise differentiation of UGS. Specifically, we maintain a consistent urban area definition across both land use cover datasets, anchored by the urban delineation provided by the MCD12Q1 dataset. However, the coarse resolution of MCD12Q1 is insufficient for detailed spatial characterization of UGS. To address this limitation, we employ the high-resolution dataset to refine the characterization of non-urban surfaces within the urban boundaries (i.e., UGS) defined by MCD12Q1. This approach yields a sophisticated land cover dataset with 10 m spatial resolution that retains the urban extent delineated by MCD12Q1 while incorporating detailed representations of UGS absent in the original dataset. Consequently, while both datasets encompass identical urban extents, the default dataset lacks representations of UGS, in contrast to the high-resolution dataset, which includes detailed depictions of UGS.

2.2 MEGANv3.1 configuration

The calculation of BVOC emissions was performed utilizing MEGANv3.1 (accessible at https://bai.ess.uci.edu/megan, last accessed: 21 November 2023). MEGAN estimates BVOC emissions as the product of an emission factor and an emission activity factor (Guenther et al., 2012a):

$$\text{Emission} = \varepsilon \cdot \gamma \cdot \rho \quad \text{(Eq. 1)}$$

In this equation, ε ($mg \cdot m^{-2} \cdot h^{-1}$) denotes an emission factor representing the emission rate under standard conditions; ρ signifies the production and consumption within the canopy, typically set as 1. The emission activity factor (γ) considers emission responses to changes in environmental and phenological conditions, and its calculation is as follows:

$$\gamma_i = C_{CE} \cdot LAI \cdot \gamma_{P,i} \cdot \gamma_{T,i} \cdot \gamma_{A,i} \cdot \gamma_{SM,i} \cdot \gamma_{C,i} \quad \text{(Eq. 2)}$$

In this equation, the activity factor for each compound class (i) denotes the emission response to light (γ_P), temperature (γ_T), leaf age (γ_A), soil moisture (γ_{SM}), Leaf Area Index (LAI), and CO_2 inhibition (γ_C). The canopy environment coefficient (C_{CE}) is assigned a value that ensures γ = 1 under standard conditions and

https://doi.org/10.5194/egusphere-2024-1163
Preprint. Discussion started: 25 June 2024

depends on the canopy environment model in use (Guenther et al., 2020a). In numerous applications of MEGAN, the activity factors for soil moisture and CO_2 inhibition were disregarded (Guenther et al., 2012a; Sindelarova et al., 2014).

Hence, the input data to drive MEGANv3.1 comprises meteorological variables (e.g., temperature, solar radiation, relative humidity, soil moisture), LAI, and three types of land cover data (i.e., ecotype, growth form, and relative vegetation composition for each ecotype/growth form). Meanwhile, the growth form datasets in MEGANv3.1 contain considerations of evergreen broadleaf forests, grasslands, and crops, which cover all types of UGS in Guangzhou city (Figure S1). Meteorological data are obtained from the WRF simulation results, and the LAI dataset is detailed in Section 2.1 as well as additional default land cover data provided by MEGANv3.1 were employed.

2.3 WRF-CMAQ and Scenario Configuration

Both the WRFv4.1.1 model and the CMAQv5.4 model are compiled and operated on a server with a Linux environment. The WRFv4.1.1 model was employed to simulate meteorological conditions, utilizing initial and boundary conditions sourced from the NCEP 1° × 1° Final (FNL) reanalysis dataset (National Centers for Environmental Prediction, National Weather Service, NOAA, U.S. Department of Commerce, 2000). As illustrated in Figure S2, four nested domains with horizontal resolutions of 27, 9, 3, and 1 km, respectively, were employed. The outermost domain encompasses mainland China, while the innermost domain zooms in Guangzhou city, and the physical parameterization configured for the WRF simulation is listed in Table S1. CMAQv5.4 utilized meteorological fields provided by WRF to model O_3 concentrations. The initial and boundary conditions for CMAQ were derived from the default profiles representing a clean atmosphere. In addition, we acquired anthropogenic emissions for the CMAQ domain from the Multi-resolution Emission Inventory for China (MEIC) 2017 developed by Tsinghua University, which contains monthly gridded (0.25° × 0.25°) emissions information for anthropogenic emissions. Moreover, CMAQ was configured with the Carbon Bond chemical mechanism (CB06) (Luecken et al., 2019) and AERO7 (Pye et al., 2017). In this study, we incorporated the Modular Emission Inventory Allocation Tools for the Community Multiscale Air Quality model (MEIAT-CMAQ, https://github.com/Airwhf/MEIAT-CMAQ, last accessed: February 27, 2024) to allocate spatial and species-specific emissions within the raw inventories, addressing discrepancies in resolution and species compared to the modeled configurations. Moreover, MEIAT-CMAQ can directly generate the hourly model-ready emission files for CMAQ via temporal allocation. The model simulation

https://doi.org/10.5194/egusphere-2024-1163
Preprint. Discussion started: 25 June 2024

spanned a month, from 21 August 2017 to 30 September 2017. To mitigate bias resulting from meteorological and chemical drift, the initial 10 days of this simulation were designated as spin-up and were not included in the analysis for this study. Given the spatial heterogeneity in the distribution of UGS across different areas, this study categorizes Guangzhou into urban, suburban, and rural regions (Figure 1). Specifically, the urban areas comprise Haizhu (HZ), Liwan (LW), Yuexiu (YX), and Tianhe (TH) districts. The suburban areas encompass Huangpu (HP), Baiyun (BY), Panyu (PY), and Nansha (NS) districts. Lastly, the rural regions include Zengcheng (ZC), Conghua (CH), and Huadu (HD) districts. To facilitate clear differentiation between the two sites in the HP region, they have been designated as HP_L and HP_H, respectively.

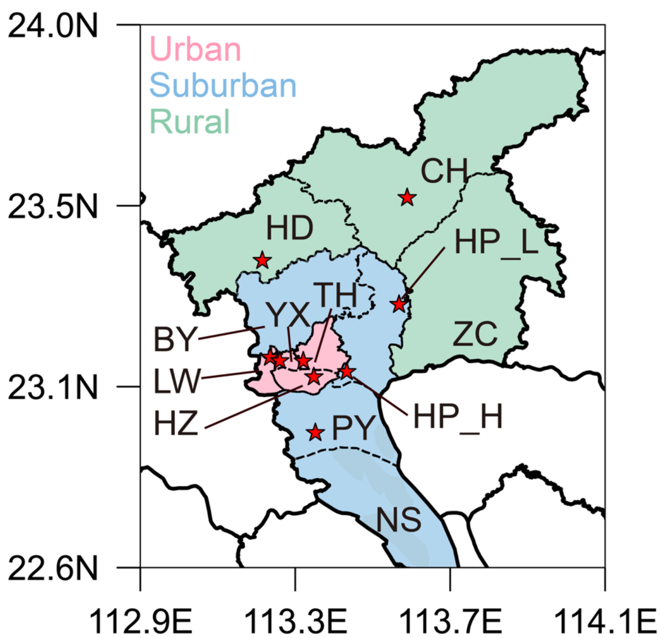

Figure 1 The innermost domain of WRF-CMAQ with various areas and the air quality station locations map.

In this study, four distinct scenarios, as listed in Table 1were established to investigate the impacts of UGS-LUCC, UGS-BVOC, and their combined effects on the ozone simulation. These scenarios also focused on the performance of the CMAQ simulation and the influence on O_3 episodes. The Gdef_N scenario considered as the base case, employs default land use cover data—specifically, data excluding UGS, and utilizes the LAI dataset with urban areas omitted (N-LAI). In contrast, the Gdef_Y scenario is similar to Gdef_N but incorporates the LAI dataset that includes urban areas (T-LAI). This adjustment allows for the assessment of the UGS-BVOC emission effects on O_3 concentrations. The Ghr_N scenario mirrors Gdef_N but differs by integrating high-resolution land use cover data, which encompasses UGS land use cover. This scenario aims to examine the UGS-LUCC effects on O_3 concentrations. Finally, the Ghr_Y scenario combines high-resolution land use cover data with the LAI dataset inclusive of urban areas, thereby enabling an exploration of the combined effects of UGS-BVOC emissions and UGS-LUCC on O_3 concentrations.

Table 1 Scenario configurations

Name	LC dataset	LAI dataset	Description
Gdef_N	Default data	N-LAI	Base
Gdef_Y	Default data	T-LAI	UGS-BVOC effects
Ghr_N	High-resolution data	N-LAI	UGS-LUCC effects
Ghr_Y	High-resolution data	T-LAI	combined effects

2.4 Observation Dataset

We utilize hourly ground-level meteorological observations, encompassing 2-m temperature (T2) and 10-m wind speed (WS10), sourced from national basic meteorological stations provided by the Guangdong Provincial Meteorological Service (Figure S3). Hourly ambient concentrations of O_3 from national monitoring stations are gathered from the China National Environmental Monitoring Centre (CNEMC). The locations of these air quality stations are depicted in Figure 1, and the air quality data and meteorological data both undergo thorough quality control. Subsequently, they are utilized to assess the model performance of WRF-CMAQ.

3. Results and discussion

3.1 Model Evaluation

Evaluation of the WRF-CMAQ model performance is undertaken through comparison against ground-level observations and the evaluation metrics of meteorological parameters are listed in Table S2, which shows that the meteorological fields were faithfully reproduced in this study and can be used to drive the air quality model.

The primary sources of isoprene (ISOP) and monoterpenes (TERP) are BVOCs, rendering the assessment of their concentrations a pivotal method for indirectly verifying the accuracy of BVOC emission estimates. Table 2 delineated within this study presents the mean concentrations of ISOP and TERP derived from various scenarios juxtaposed with the observed average concentrations. This comparative analysis reveals that after the incorporation of UGS-BVOC emissions, there is an augmentation in the ISOP concentration from 0.24 ppb to 0.31 ppb and from 0.21 ppb to 0.28 ppb under distinct land use cover scenarios (Gdef and Ghr), relative

https://doi.org/10.5194/egusphere-2024-1163
Preprint. Discussion started: 25 June 2024

to an observed concentration of 0.33 ppb. This increment signifies a substantial diminution in the discrepancy between the modeled and observed concentrations attributable to UGS-BVOC emissions. Analogously, the integration of UGS-BVOC emissions yields a refinement in the estimation accuracy of ISOP concentrations at both Modiesha and Wanqinsha sites, as evidenced by a reduced bias.

These findings reveal that ISOP concentrations are underestimated by 26.19%-36.36% when UGS-BVOCs are excluded. Specifically, this range represents the proportion of ISOP originating from UGS-BVOCs. Moreover, numerous studies highlight the significant role of ISOP in ozone formation within the Pearl River Delta (PRD) region, including Guangzhou. For instance, Zheng et al., (2009) demonstrated that ISOP has the highest ozone formation potential among all VOCs. Therefore, incorporating UGS-BVOCs into ISOP concentration estimates is crucial for accurately modeling regional ozone levels.

Table 2 Evaluation of ISOP concentrations.

Location	Observed period	observed concentration (ppb)	Gdef_N (ppb)	Gdef_Y (ppb)	Ghr_N (ppb)	Ghr_Y (ppb)	Reference
Modiesha (urban) 23.11N, 113.33E	20 Sep. 2017 – 20 Nov. 2017	0.33	0.24	0.31	0.21	0.28	Meng et al., (2022)
Wanqinsha (suburban) 22.43N, 113.33E	20 Sep. 2017 – 20 Nov. 2017	0.42	0.31	0.38	0.27	0.35	Meng et al., (2022)

Additionally, various statistical metrics were utilized to assess the performance of NO_2 and O_3 concentrations from CMAQ simulation (Emery et al. 2017). These metrics comprise the correlation coefficient (R), normalized mean bias (NMB), and normalized mean error (NME). The formulas for these metrics are listed in Table S3. Emery et al. (2017) propose that the model performs acceptably when NMB and NME of hourly O_3 concentrations are less than 15% and 25%, respectively, and the correlation coefficient (R) is greater than 0.5. As illustrated in Table 3, it is evident that all the scenarios exceed the specified requirement, albeit with some degree of underestimation. Despite these discrepancies, the model demonstrates sufficient reliability and can be effectively utilized in subsequent research. In addition, we also evaluate the simulation performance for NO_2 in each scenario and the results suggest that all models have R above 0.63, and while there is some overestimation, the NMB is 15.0%, 15.2%, 13.0%, and 13.2% for Gdef_N, Gdef_Y, Ghr_N, and Ghr_Y, respectively. It should be emphasized that integrating UGS-BVOC into the modeling process can slightly improve the accuracy of NO_2 predictions, reducing the MB from 7.01 $\mu g/m^3$ to 6.94 $\mu g/m^3$, and from 6.09 $\mu g/m^3$ to 6.03 $\mu g/m^3$ for Gdef and Ghr scenarios, respectively.

https://doi.org/10.5194/egusphere-2024-1163
Preprint. Discussion started: 25 June 2024

Table 3: The evaluation results for each scenario.

Pollutant		Sim (μg/m^3)	Obs(μg/m^3)	MB(μg/m^3)	NMB	NME	R
O_3	Gdef_N	60.49	65.33	-4.84	-6.7%	23.6%	0.82
	Gdef_Y	61.43	65.33	-3.90	-5.3%	23.6%	0.82
	Ghr_N	61.91	65.33	-3.42	-4.8%	22.5%	0.83
	Ghr_Y	62.86	65.33	-2.47	-3.4%	22.4%	0.83
NO_2	Gdef_N	53.09	46.07	7.01	15.2%	45.7%	0.63
	Gdef_Y	53.02	46.07	6.94	15.0%	45.5%	0.63
	Ghr_N	52.17	46.07	6.09	13.2%	43.8%	0.63
	Ghr_Y	52.11	46.07	6.03	13.0%	43.6%	0.63

In terms of O_3, the UGS-BVOC, UGS-LUCC, and combined effects have various performances in different regions (Table 4). These results indicate that the inclusion of UGS-BVOC emissions significantly influences MDA8 O_3 concentrations in urban regions and this effect, primarily observed when comparing the Gdef_Y with Gdef_N and Ghr_Y with Ghr_N scenarios, is largely due to the VOC-limited areas prevalent in Guangzhou (He et al., 2024). By integrating the UGS-BVOC emissions into the models (comparing Gdef_Y and Gdef_N scenarios), the bias in all regions, including a notable improvement in the urban region from -7.77 μg/m³ to -1.60 μg/m³, is reduced. Additionally, the UGS-BVOC emissions slightly enhance R values in the urban and suburban regions, indicating a more accurate MDA8 O_3 trend representation. The UGS-LUCC (land use and land cover change) effects, as seen when comparing Ghr_N and Gdef_N scenarios, also significantly improve model biases and the combined effects of both UGS-BVOC and UGS-LUCC (comparing Ghr_Y and Gdef_N scenarios) substantially ameliorate model biases in the urban and suburban regions.

Table 4 The evaluation results for O_3 in various regions.

	MB (μg/m^3)				R			
Regions	Gdef_N	Gdef_Y	Ghr_N	Ghr_Y	Gdef_N	Gdef_Y	Ghr_N	Ghr_Y
Urban	-7.773	-4.803	-4.523	-1.600	0.805	0.810	0.810	0.813
Suburban	-8.737	-6.967	-6.880	-5.093	0.737	0.743	0.717	0.727
Rural	-10.950	-10.195	-10.430	-9.705	0.665	0.655	0.695	0.690

3.2 Estimation of UGS-BVOC emissions under different land use cover

This study comprehensively summarizes the UGS-BVOC emissions across various species for all regions in Guangzhou City in September. Given that the variances in the UGS-BVOC emissions due to different land use covers are relatively minor, the primary Table 5 presents emissions driven by the default land use cover. For a detailed breakdown of emissions attributable to varied land use covers, refer to Table S4. A review of the data reveals that monoethylene (TERP) and isoprene (ISOP) rank as the highest emitting species with proportions are 20.46% and 31.91% in this study, respectively, aligning with the findings of previous studies

https://doi.org/10.5194/egusphere-2024-1163
Preprint. Discussion started: 25 June 2024

(Cao et al., 2022; Guenther et al., 2012b). Furthermore, Table 5 reveals that in September, the suburban region registered the highest UGS-BVOC emissions in Guangzhou, peaking at 367.31 Gg. This is followed closely by the rural and urban regions, recording emissions of 173.65 Gg and 125.53 Gg, respectively.

Table 5 The summarized table of UGS-BVOC emissions in Guangzhou city in September via default land use cover (units: Gg).

Species	Abbreviations	Urban (Gg)	Suburban (Gg)	Rural (Gg)	Total (Gg)
Acetic acid	AACD	0.86	2.44	1.18	4.48
Acetaldehyde	ALD2	3.46	11.57	5.83	20.86
Formaldehyde	FORM	0.95	3.90	2.17	7.02
Methanol	MEOH	12.47	41.31	20.36	74.14
Formic acid	FACD	2.79	7.84	3.79	14.42
Ethane	ETHA	2.12	8.40	4.64	15.16
Ethanol	ETOH	3.63	12.13	6.11	21.87
Acetone	ACET	6.22	21.52	11.63	39.37
Propane	PRPA	2.08	8.21	4.54	14.83
Ethene	ETH	3.97	15.64	8.64	28.25
Isoprene	ISOP	47.30	117.32	48.06	212.68
Monoterpenes	TERP	24.07	74.85	37.51	136.43
Alpha pinene	APIN	11.26	30.07	13.16	54.49
Methane	ECH4	0.04	0.14	0.08	0.26
Sesquiterpenes	SESQ	4.31	11.97	5.95	22.23
Total	Total	125.53	367.31	173.65	666.49

Figure 2 (A) provides a detailed illustration of the UGS-BVOC emissions across various regions in Guangzhou City, driven by default land use cover data, and compares these with the estimates derived from high-resolution land use cover data, which presents that the suburban region exhibits the highest UGS-BVOC emissions among the three studied regions, totaling 413.47 Gg. This predominance is linked to the larger extent of UGS in the suburban region, as depicted in Figure 5(A), while the emissions in urban and rural regions are reported at 137.69 Gg and 198.64 Gg, respectively. Moreover, UGS-LUCC is instrumental in modulating BVOC emissions, leading to an uptick in urban and rural regions while precipitating a decline in the suburban region. Notably, a slight increase in solar radiation (SOL_RAD) by 0.05% (Figure 2 (C)), attributable to a reduced urban fraction in the Ghr dataset, results in augmented solar exposure. Concurrently, a marginal reduction in surface temperature (SFC_TMP) by 0.02% (Figure 2 (D)), facilitated by increased vegetation albedo cooling effects, underpins the decrease in UGS-BVOC emissions within suburban regions. This phenomenon underscores the critical role of lowered SFC_TMP—driven by vegetation's higher albedo—in curtailing emissions stemming from UGS-LUCC. Moreover, in urban contexts, the diminished urban fraction enhances SOL_RAD and SFC_TMP, promoting higher emissions, a trend mirrored to a lesser extent in the rural region following the update of land use cover data to Ghr. Figure 2 (B) offers a clear depiction of the proportion of

https://doi.org/10.5194/egusphere-2024-1163
Preprint. Discussion started: 25 June 2024

UGS-BVOC emissions relative to natural area BVOC emissions in each region of Guangzhou City, which presents that the UGS-BVOC emissions in urban regions constitute 57.34% of the total BVOC emissions in this region because of the larger urban proportions in the urban region (Figure 5), while the UGS-BVOC emission proportion in suburban and rural are 19.44% and 1.86% respectively. This indicates a significant contribution of the UGS-BVOC emissions in the urban region. Furthermore, when examining the relative differences in the BVOC emissions resulting from various land use covers across the city, the changes are found to be minimal, which suggests that meteorological alterations from land use cover do not majorly influence the proportion of the UGS-BVOC emissions emanating in Guangzhou. Thus, factors other than land use changes might be more critical in shaping the distribution and intensity of the UGS-BVOC emissions in urban settings.

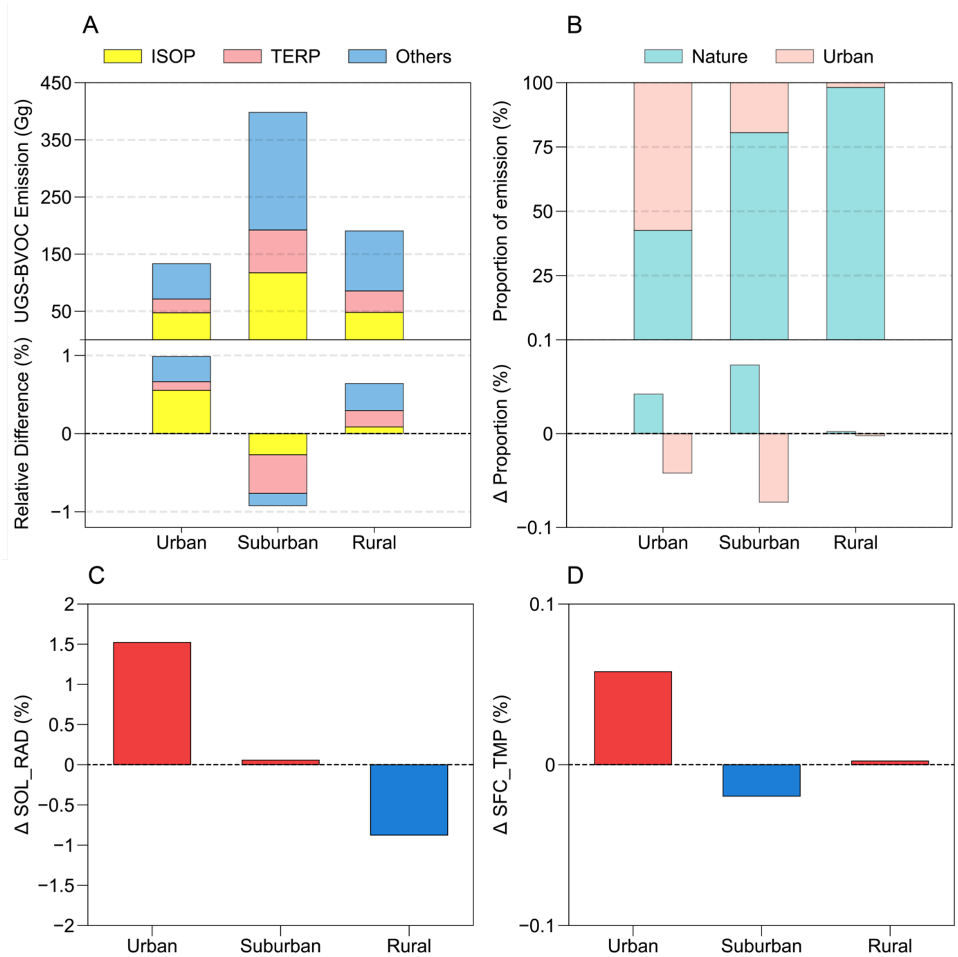

Figure 2 The UGS-BVOC emissions of each species and relative difference (Ghr - Gdef) from various land use cover (a), the proportion of emissions from urban and nature and the relative proportion difference (Ghr - Gdef) from various land use cover (b), the relative difference of solar radiation (C), and surface temperature (D) driven via various land use cover datasets.

https://doi.org/10.5194/egusphere-2024-1163
Preprint. Discussion started: 25 June 2024

Figure 3 (A) and (B) collectively highlight the patterns of the UGS-BVOC emissions across different land use covers, pinpointing the emission hotspots in urban and suburban regions, which effectively illustrate how land use cover influences the UGS-BVOC emissions in various parts of the city. Additionally, Figure 3 (C) delves into the disparities in the UGS-BVOC emissions attributed to different land use cover datasets. It reveals that the variations in emissions are predominantly concentrated in the identified hotspots. Moreover, Figure 3 (C) indicates that employing high-resolution land cover data typically results in marginally higher estimates of the UGS-BVOC emissions, with an increase ranging between 0.8% to 2.9%. Figure 5 (E) and (F) illustrate that despite a marginal reduction in solar radiation within urban locales, a corresponding minor temperature elevation modestly boosts UGS-BVOC emissions, which presents that the increase in temperature from UGS-LUCC causes the rise of the UGS-BVOC emissions.

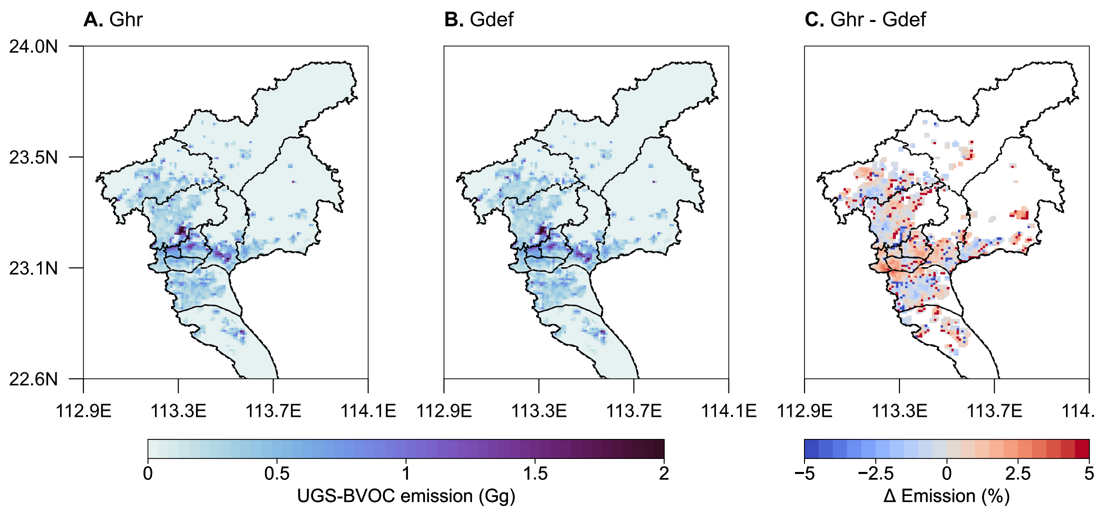

Figure 3 The UGS-BVOC emission maps from default (A) and high-resolution (B) land use cover, and the differences of various UGS-BVOC emissions (C).

As illustrated in Figure S1, UGS in Guangzhou comprises three primary types of vegetation: evergreen broadleaf forests, which are composed of Evergreen Broadleaf Trees (EBTs), cropland, and grasslands. This classification has enabled a more nuanced understanding of how different types of UGS vegetation influence UGS-BVOC emissions. Figure 4 reveals that EBTs predominate the urban vegetation landscape in Guangzhou and are associated with higher rates of UGS-BVOC emissions as their coverage increases. Conversely, an increase in the proportion of cropland correlates with reduced UGS-BVOC emissions, highlighting its minimal contribution to the overall UGS-BVOC emissions of Guangzhou. Grasslands exhibit a variable impact on BVOC emissions; when they constitute over 80% of the UGS, the emission rates are relatively low. However,

https://doi.org/10.5194/egusphere-2024-1163
Preprint. Discussion started: 25 June 2024

when grassland coverage ranges between 60-80%, its BVOC emissions surpass those from cropland within the same percentage range. Overall, EBTs emerge as the primary contributors to UGS-BVOC emissions, with grasslands and croplands making lesser contributions.

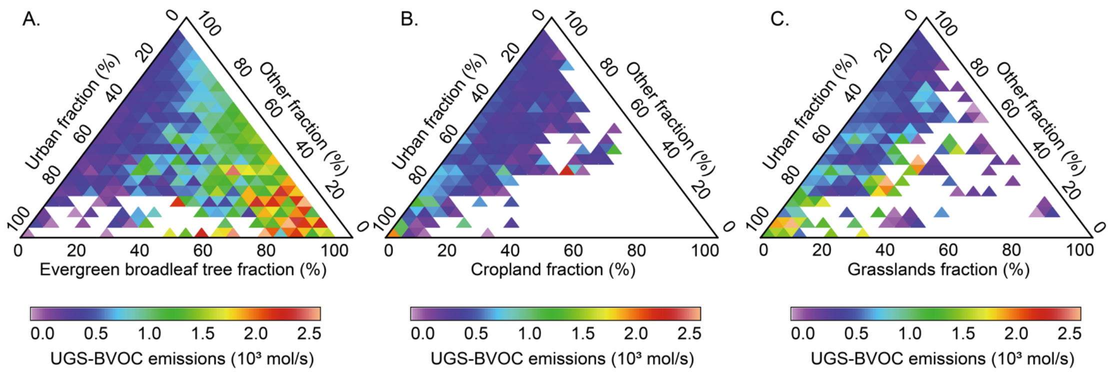

Figure 4 Ternary heat map for various vegetation in UGS with the UGS-BVOC emission rate and the invalid value in this figure represents no UGS-BVOC emission.

In addition to the proportion of UGS, the UGS-BVOC emissions in Guangzhou city are significantly influenced by meteorological factors such as surface temperature and solar radiation (Guenther et al., 2020b). To elucidate the spatial heterogeneity of the UGS-BVOC emissions, this study analyzes variations in these key factors. The simulation results depicted in Figure 5 (A) show the distribution pattern of UGS, which are predominantly located in the urban region, which account for a higher percentage of the UGS-BVOC emissions compared to others. Interestingly, as indicated in Figure 5 (B), the urban region receives less solar radiation than other regions likely due to the shading effect of urban canopies. Conversely, the urban region exhibits elevated temperatures attributable to the urban heat island effect, leading to an increase in UGS-BVOC emissions. Thus, while the distribution of UGS contributes to the variation in the UGS-BVOC emissions across different regions, the more significant factor is the enhanced UGS-BVOC emission due to higher temperatures in densely urbanized areas. The spatial dynamics of the UGS-BVOC emissions are significantly shaped by two key meteorological factors: solar radiation and surface temperature. These elements independently play a crucial role in determining both the spatial pattern and the intensity of the UGS-BVOC emissions. Solar radiation directly influences the rate of photosynthesis and, consequently, the production of BVOCs, while temperature affects not only the physiological processes of vegetation but also the volatilization rate of these compounds (Fuhrer et al., 1997; Lombardozzi et al., 2014). The intricate interplay between these factors leads to spatial variations in the UGS-BVOC emissions, with areas receiving higher solar radiation and experiencing warmer temperatures typically exhibiting more intense BVOC

https://doi.org/10.5194/egusphere-2024-1163
Preprint. Discussion started: 25 June 2024

emissions.

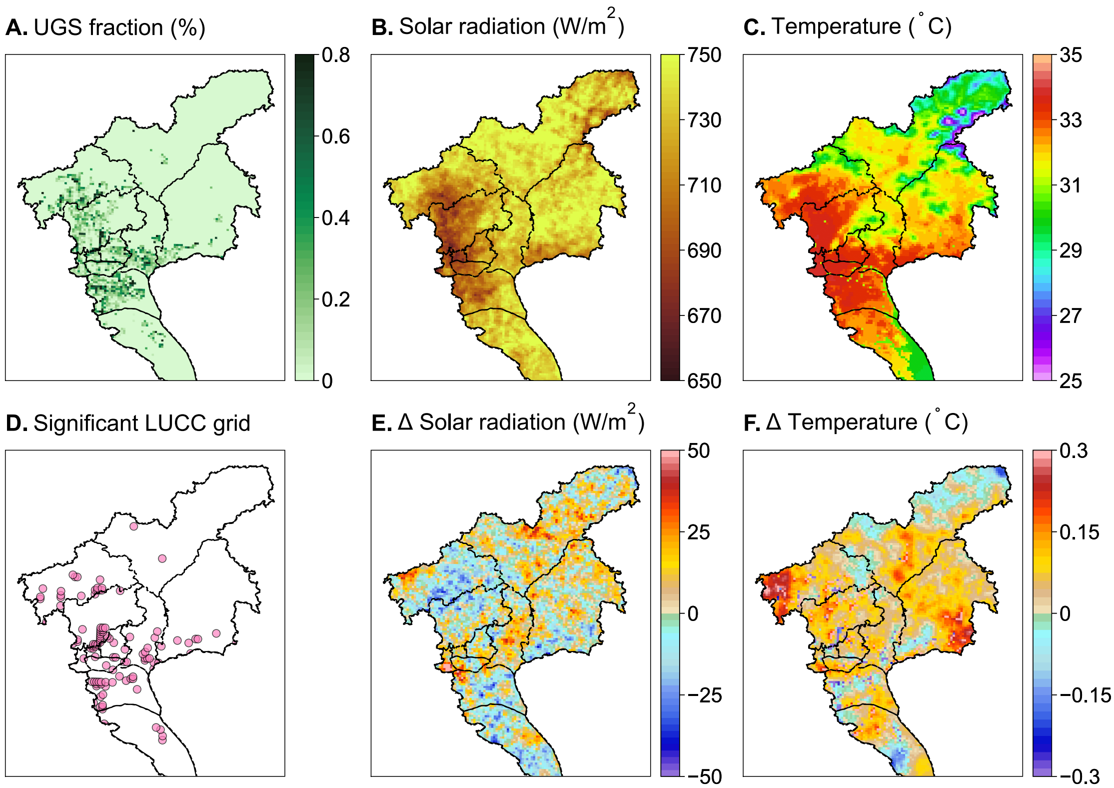

Figure 5 The UGS map (A) and the meteorological fields from the Ghr_N scenario (B and C). (D) is the grid locations where the land use experienced significant changes, (E) and (F) are the differences in solar radiation and temperature in various land use cover data (Ghr - Gdef).

This section has conclusively demonstrated that during the high O_3 season (September) in Guangzhou, the contribution of UGS-BVOC is substantial and cannot be overlooked and a notable finding is the strong spatial heterogeneity in these emissions across the city. The analysis also highlights high-resolution land use cover data increase the estimation of the UGS-BVOC emissions in the urban and suburban regions.

3.3 Impact of UGS-LUCC and UGS-BVOC on Ozone Concentrations

The study evaluates the effects of UGS-BVOC and UGS-LUCC on MDA8 O_3 concentrations in Guangzhou, both individually and in combination. The analysis reveals that the UGS-BVOC emissions alone (Figure 6 A) primarily affect urban areas, significantly increasing MDA8 O_3 concentrations by 2.2-3.0 μg/m³ (+2.3-3.2%), which increment aligns with findings from Los Angeles, where Schlaerth et al., (2023) reported a contribution of 2.5 μg/m³ from UGS-BVOC to urban MDA8 O_3 levels. In contrast, the sole impact of the UGS-LUCC

https://doi.org/10.5194/egusphere-2024-1163
Preprint. Discussion started: 25 June 2024

effects (Figure 6 B) is more extensive, influencing both urban and suburban regions and resulting in a general increase of approximately 2.3-4.2 μg/m³ (+2.3-4.3%) in MDA8 O_3 levels, which can be attributed to the higher temperature and solar radiation (Figure 5 (E)-(F)). In Guangzhou, the transformation of urban surfaces to natural vegetation due to UGS-LUCC results in lower albedo and consequently lower temperatures. However, this change also reduces the height of the urban canopy, diminishing its shading effects on solar radiation and paradoxically leading to higher temperatures in some regions. Therefore, considering the UGS-LUCC effect, the decreased urban canopy height could lead to elevated temperatures, thereby potentially increasing ozone production. However, the most significant results emerge under the combined effect of UGS-BVOC and UGS-LUCC (Figure 6 C), where a substantial increase in O_3 concentration, ranging from 3.6-8.0 μg/m³ (+3.8-8.5%), is observed across both urban and suburban areas. The observed increase highlights the critical influence of UGS-BVOC emissions and UGS-LUCC on ozone levels, underlining the impossibility of overlooking these factors in ozone concentration research. This revelation points to the essential role that integrated urban planning and environmental management play in controlling ozone pollution within metropolitan regions.

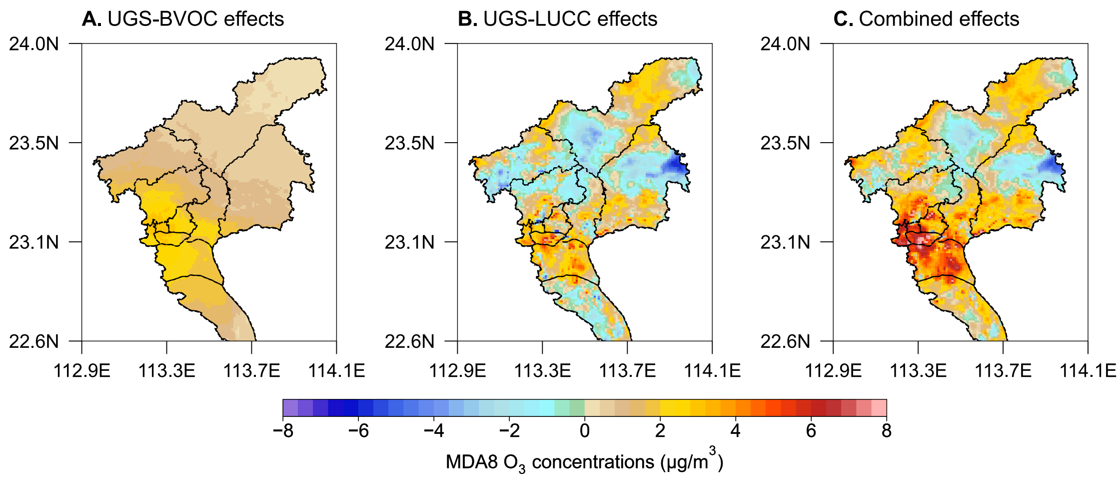

Figure 6 The map of UGS-BVOC effects (a), LUCC effects (b), and combined effects (c) in MDA8 O_3.

Previous studies have established that O_3 episodes are often accompanied by high temperatures and intense solar radiation, conditions that can exacerbate the UGS-BVOC emissions, critically affecting air quality model performance (Shan et al., 2023; Soleimanian et al., 2023). In this study, an O_3 episode is defined as a period of two or more consecutive days with maximum daily average 8-hour (MDA8) O_3 concentrations exceeding 160 μg/m³ (Wu et al., 2020). Our analysis, as depicted in Figure 7 (A), identified two such episodes in Guangzhou City during September: the first from September 16 to 21 and the second from September 26 to 28. The Gdef_N scenario successfully captures these episodes but tends to underestimate both MDA8 O_3

https://doi.org/10.5194/egusphere-2024-1163
Preprint. Discussion started: 25 June 2024

during these episodes. Figure 7 (B) and (C) highlight a notable reduction in wind speed during both episodes, particularly during the second episode. Despite some diffusion enhancement due to increased PBLH with rising surface temperatures (Figure S4), the surface temperature hike concurrently fosters O_3 production. Consequently, the episodes were dominated by a combination of temperature increases, which elevated O_3 concentrations, and wind speed decreases. Furthermore, Figure 7 (C) illustrates that there was a significant spike in carbon monoxide (CO) concentrations during these episodes. CO, often used as a tracer in studies, indicates the worsening of diffusion conditions, leading to the accumulation of NO_2 - a primary O_3 precursor - thereby culminating in O_3 episodes in Guangzhou city.

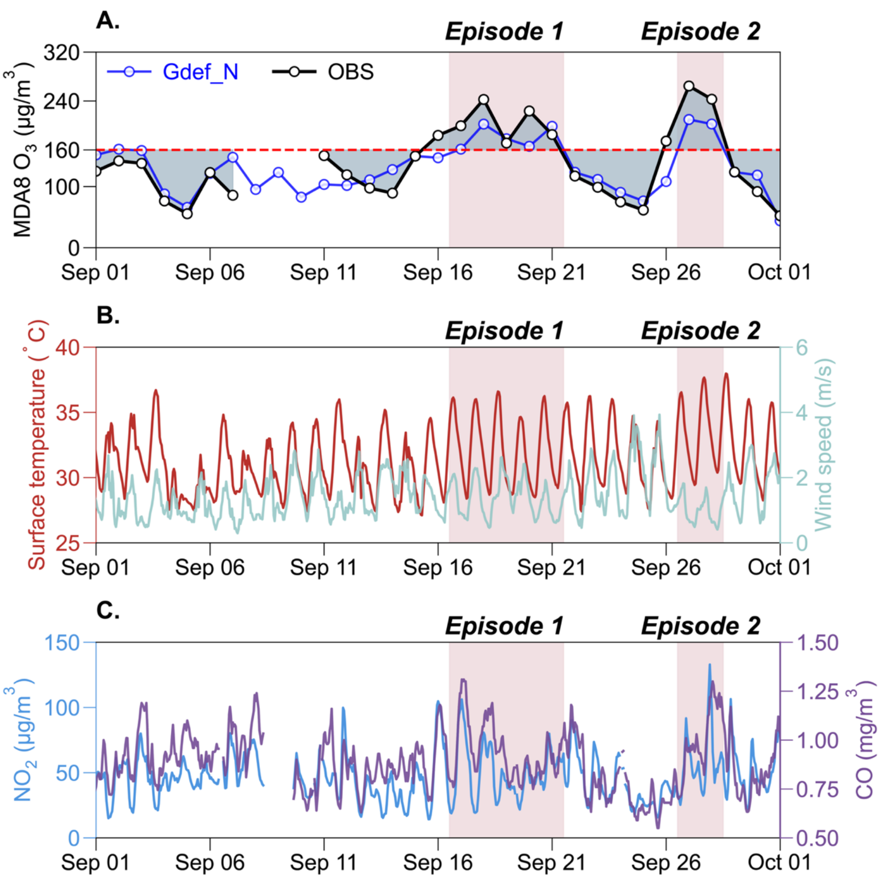

Figure 7 The comparison between the average values from simulation results grids which have air quality stations produced by the Gdef_N scenario and the average observation values for MDA8 O_3 (A). (B) are the meteorological fields from the average values from the simulation result grids, which have the same locations as the air quality stations. (C) are the observed average values for NO_2 and CO concentrations from all air quality stations.

Figure 8 presents that in assessing the simulation of O_3 episodes, the Gdef_N scenario, which initially underestimated O_3 concentrations, prompted an evaluation of improvements using different scenarios: UGS-

https://doi.org/10.5194/egusphere-2024-1163
Preprint. Discussion started: 25 June 2024

LUCC (Ghr_N), UGS-BVOC emissions (Gdef_Y), and a combination of both (Ghr_Y). The analysis, focusing on urban, suburban, and rural stations, reveals that all scenarios tend to underestimate O_3 levels between both episodes. However, incorporating the UGS-BVOC emissions into the model results in a notable increase in mean simulated MDA8 O_3 concentrations, particularly in urban and suburban areas. For urban sites, the mean simulated MDA8 O_3 increased by +3.2 and +6.3 μg/m³ (+1.8% and +3.3%, respectively), while for suburban sites, the increase was +2.0 μg/m³ (+1.1%) and +3.3 μg/m³ (+1.9%), with rural sites experiencing a smaller increase of only +1.0 μg/m³ (+0.5%) and +1.1 μg/m³ (+0.7%). This trend indicates a more pronounced impact in urban and suburban areas compared to rural. Notably, the influence of the UGS-BVOC emissions on MDA8 O_3 in Episode 2 (+6.3 μg/m³) was significantly greater than in Episode 1 (+3.2 μg/m³), suggesting that meteorological conditions in Episode 2 were more conducive to the UGS-BVOC emissions, particularly in urban areas, which usually is VOC-limited areas.

In Episode 1, the UGS-LUCC effects on O_3 concentrations were comparable to that of UGS-BVOC emissions, but in Episode 2, the UGS-LUCC effects led to a near doubling of urban MDA8 O_3 increase by 12.1 μg/m³ (+6.48%) compared to the UGS-BVOC emissions. This indicates that the UGS-LUCC effects play a non-negligible role in O_3 pollution studies, and the response to such changes under different meteorological conditions varies significantly. Furthermore, due to the limited proportion of UGS in suburban and rural areas, the increased effect of UGS on O_3 is less pronounced in these regions, and nearly negligible in Episode 2. While the UGS-BVOC emissions alone have a modest effect on O_3 concentrations, their impact can become significant when combined with the UGS-LUCC effects. For instance, the combined effects in the urban region increased by 6.6 μg/m³ (+3.7%) and 18.7 μg/m³ (+10.0%) during Episode 1 and Episode 2, respectively.

https://doi.org/10.5194/egusphere-2024-1163
Preprint. Discussion started: 25 June 2024

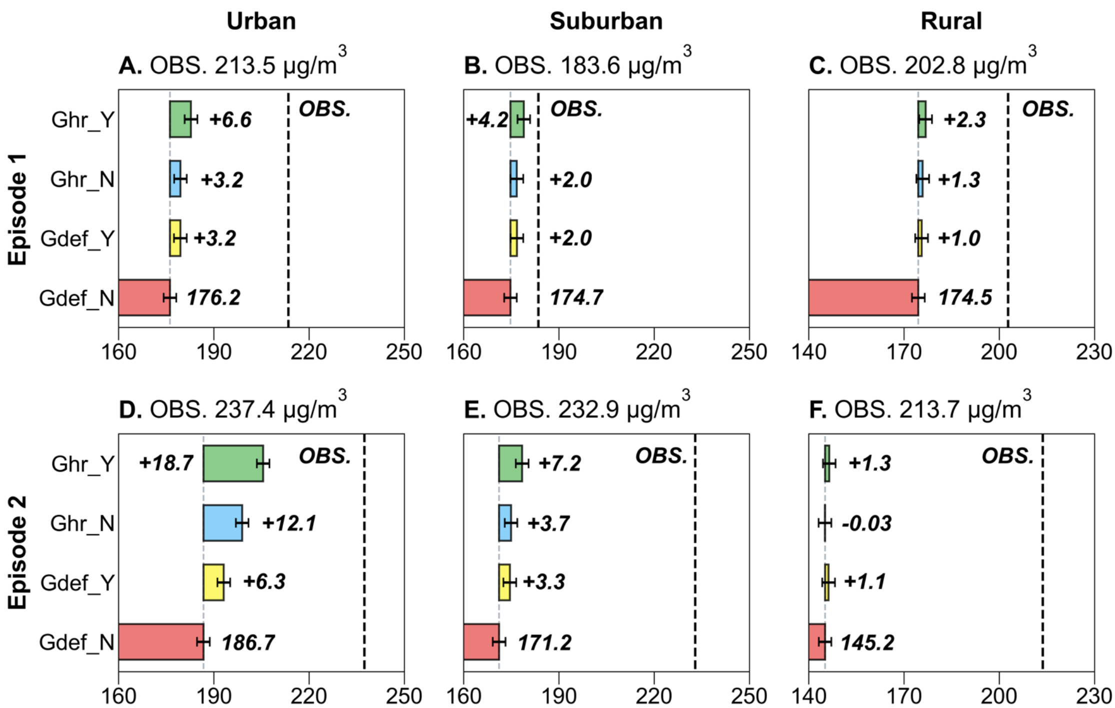

Figure 8 Comparison of simulated versus observed mean MDA8 O_3 concentrations across different scenarios for two episodes. The figure is organized into columns representing urban (4 sites), suburban (3 sites), and rural (2 sites) settings (columns 1-3, respectively) and rows indicating comparisons for episode 1 and episode 2 (rows 1 and 2, respectively).

Figure 9 presents the map of each effect on MDA8 O_3 in both episodes and the influence of UGS-BVOC emissions (Figure 9 (A) and (D)) on the MDA8 O_3 concentration during Episode 1 and Episode 2 ranges from 0 to 4.27 μg/m³ and 0 to 7.43 μg/m³, respectively, with urban areas witnessing the most significant impact. This variance can be primarily ascribed to the heightened temperatures during Episode 2 (Figure 7 (B)), which create conditions more conducive to ozone generation through UGS-BVOC emissions. Furthermore, the UGS-LUCC effect's maximal contribution to the urban MDA8 O_3 levels could escalate to 4.62 μg/m³ in Episode 1 and 50.90 μg/m³ in Episode 2 while the cumulative effects of UGS-LUCC and UGS-BVOC emissions are projected to enhance MDA8 O_3 concentrations to 10.31 μg/m³ and 53.93 μg/m³ for the respective episodes. This marked increase in the episodes' contributions can be linked to the differential responsiveness of land use data under various meteorological conditions. Notably, while the contribution from the UGS-BVOC effect during Episode 2 substantially exceeds that of Episode 1, the incremental impact of UGS-LUCC on combined effects in Episode 2 is notably smaller than in Episode 1. This phenomenon indicates that the escalated UGS-BVOC emissions in Episode 2 may start to inhibit ozone production rates incrementally.

https://doi.org/10.5194/egusphere-2024-1163
Preprint. Discussion started: 25 June 2024

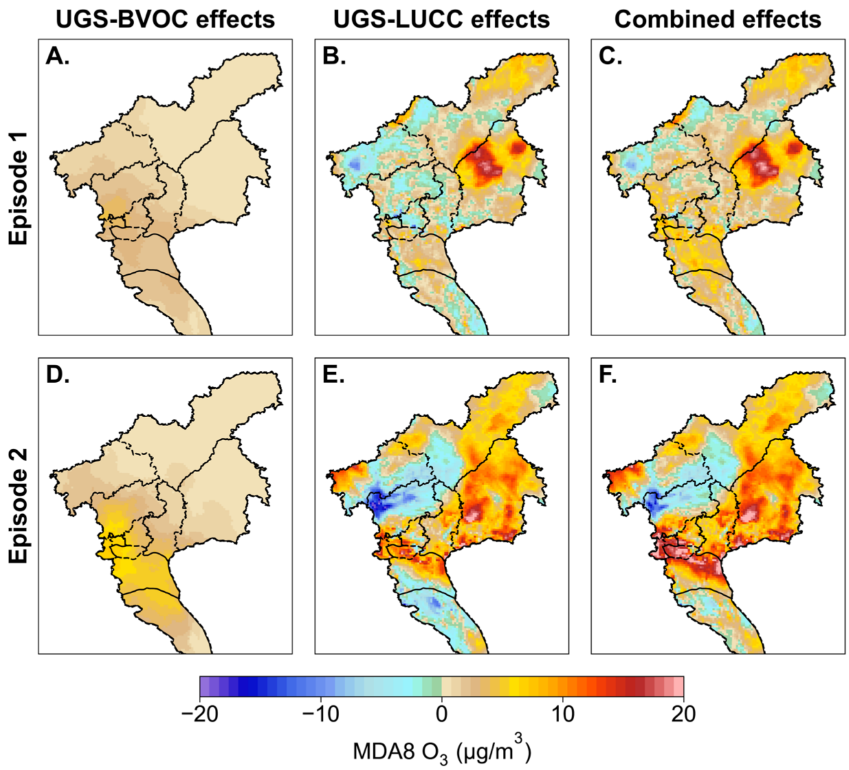

Figure 9 The UGS-BVOC effects (A, D), the UGS-LUCC effects (B, E), and the combined effects (C, F) in Episode 1 and Episode 2, respectively.

Figure 8 reveals that both observed O_3 episodes were primarily caused by reduced diffusion conditions. Notably, the impact of the UGS-LUCC effects varied significantly between the two episodes. Analysis of meteorological variables, specifically wind speed and PBLH, which are crucial for diffusion, demonstrate distinct patterns. Figure 10 illustrates that during Episode 1, the UGS-LUCC effects led to a notable increase in the frequency of wind speeds at 1.2-1.4 m/s, while simultaneously reducing the frequency at 0.9-1.1 m/s, which indicates an overall increase in wind speed due to the UGS-LUCC effects during Episode 1. In contrast, Episode 2 experiences a significant decrease in wind speed frequency at 0.7-1.1 m/s, with an increase in the lower range of 0.5-0.7 m/s. This suggests that the UGS-LUCC effects further reduce the already low wind speeds in Episode 2. Concerning PBLH, the UGS-LUCC effects are observed to elevate PBLH during Episode 1, which led to a decrease in PBLH during Episode 2. Therefore, the UGS-LUCC effects are markedly more pronounced in Episode 2 than in Episode 1, contributing to a more substantial alteration of meteorological conditions affecting air dispersion and, consequently, O_3 formation.

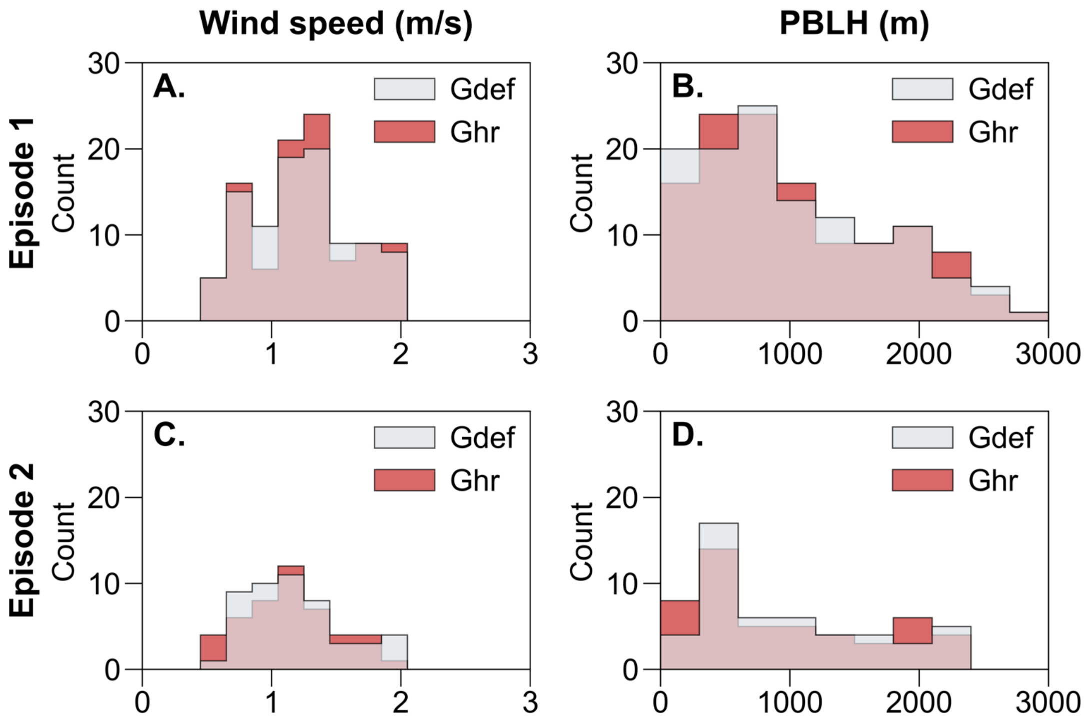

Figure 10 The frequency of wind speed (column 1) and PBLH (column 2) in Episode 1 (row 1) and Episode 2 (row 2) driven by different land use cover datasets.

4. Conclusion

The rapid urbanization process was accompanied by a higher frequency of ozone episodes. It has been increasingly recognized that UGS can potentially exacerbate ozone pollution under specific conditions due to the UGS-LUCC and UGS-BVOC emissions. Guangzhou, located in the South of China, a pioneer city reform and opening up, has experienced rapid urbanization over the past thirty years, accompanied by the challenge of ozone pollution. Despite efforts to reduce anthropogenic emissions, ozone episodes occur with relatively high frequency in Guangzhou. This study selected September 2017, a month with a high incidence of ozone episodes in Guangzhou, to estimate the UGS-BVOC emissions using the WRF-MEGAN model and quantitatively assess the impact of UGS-LUCC, UGS-BVOC, and their combined effects on two ozone episodes in September 2017 using the CMAQ model. The major findings are shown as follows.

1. In September 2017, the UGS-BVOC emissions in Guangzhou totaled 666.49 Gg, with ISOP and TERP as the primary species, emitting 212.68 and 136.43 Gg, respectively. Spatially, UGS-BVOC emissions

https://doi.org/10.5194/egusphere-2024-1163
Preprint. Discussion started: 25 June 2024

were predominantly located in urban areas, attributed to the more extensive distribution of UGS there. The study also indicates that meteorological changes caused by UGS-LUCC do not significantly affect UGS-BVOC emissions. Instead, the formation of emission spatial distribution and intensity is closely related to local surface temperature and solar radiation. This understanding underscores the importance of considering local solar radiation and temperature conditions when assessing and modeling the distribution of the UGS-BVOC emissions, as they are pivotal in driving the spatial characteristics of these emissions. Moreover, EBTs, which are the main vegetation type in the UGS of Guangzhou and a significant source of UGS-BVOCs, provide a reference for future urban greening in the city to select species with lower emission factors as the primary vegetation types.

2. Considering UGS-BVOC and UGS-LUCC can effectively mitigate the underestimation of surface ozone concentrations by regional air quality models. For instance, incorporating UGS-BVOC emissions results in an increase in ISOP concentration from 0.24 ppb to 0.31 ppb and from 0.21 ppb to 0.28 ppb under different land use scenarios (Gdef and Ghr), compared to a baseline concentration of 0.33 ppb. This significant enhancement in ISOP concentrations—the predominant component in BVOCs and the most crucial VOC for O_3 formation in the PRD—highlights two key points. Firstly, it indicates an improvement in the accuracy of BVOC concentration simulations. Secondly, this precise estimation of BVOCs has notably shifted the MB of O_3 simulations from 7.77 μg/m³ to -1.60 μg/m³ in urban areas. Additionally, the simulation of NO_2 concentrations also shows slight improvements, with the MB decreasing from 7.01 μg/m³ to 6.03 μg/m³ upon accounting for UGS-BVOCs and UGS-LUCC. Given that the UGS are often located in densely populated urban regions, their inclusion in air quality simulations is crucial for accurately modeling urban air quality.
3. The UGS-BVOC emissions have a significant impact on ozone concentrations, with increases ranging from 2.2-3.0 μg/m³ in urban regions, However, when considering the combined UGS-LUCC and UGS-BVOC effects, the impact on MDA8 O_3 concentrations becomes significant, with values ranging from 3.6-8.0 μg/m³ in urban regions. This indicates the importance of considering both UGS-LUCC and UGS-BVOC impacts when discussing the influence of UGS on air quality. Since UGS exhibits different effects in various ozone episodes, it is found that the impact of UGS on ozone levels is related to specific meteorological conditions. In the episodes of this study, the combined effects on MDA8 O_3 can reach up to 18.7 μg/m³ in urban regions.

This study on ozone pollution in Guangzhou provides key insights for other cities on integrating UGS with air quality management. By including UGS-BVOC emissions and UGS-LUCC in the air quality model, the

https://doi.org/10.5194/egusphere-2024-1163
Preprint. Discussion started: 25 June 2024

study demonstrates improved accuracy in predicting surface ozone concentrations, which can aid urban planners and environmental policymakers in refining their strategies to better address urban air pollution. Moreover, these findings encourage cities to integrate urban forestry into their land use planning and air quality frameworks, promoting environmental sustainability amid rapid urbanization.

Data availability

Model output data used for analysis and plotting, and the code used for simulations can be made available upon request (Haofan Wang, wanghf58@mail2.sysu.edu.cn).

Author contributions

HFW conceived the study, carried out the model simulations, and drafted the manuscript. YJL and THZ completed the data visualization. YML conceived and supervised this study, and reviewed and edited the paper. XL and YZ provided useful comments on the paper. QF supervised and funded the study. CS provided the meteorological data for model evaluation.

Competing interests

The contact author has declared that neither they nor their co-authors have any competing interests.

Acknowledgment

The authors would like to thank the MEIC team from Tsinghua University for providing the anthropogenic emissions for this study. Meanwhile, we also thank Tianhe-2 for providing the computer resources.

Financial support

This work is jointly funded by the innovation Group Project of Southern Marine Science and Engineering Guangdong Laboratory (Zhuhai) (316323005), Guangdong Basic and Applied Basic Research Foundation (2020B0301030004, 2023A1515110103, 2023A1515010162), National Natural Science Foundation of China

https://doi.org/10.5194/egusphere-2024-1163
Preprint. Discussion started: 25 June 2024

(42105097, 42075181, 42375182), Guangdong Science and Technology Planning Project (2019B121201002), and Science and Technology Planning Project of Guangzhou (2023A04J1544).

Reference

Allen, M.R., Ingram, W.J., 2002. Constraints on future changes in climate and the hydrologic cycle. Nature 419, 224–232. https://doi.org/10.1038/nature01092

Arghavani, S., Malakooti, H., Bidokhti, A.A., 2019. Numerical evaluation of urban green space scenarios effects on gaseous air pollutants in Tehran Metropolis based on WRF-Chem model. Atmos. Environ. 214, 116832. https://doi.org/10.1016/j.atmosenv.2019.116832

Burnett, R., Chen, H., Szyszkowicz, M., Fann, N., Hubbell, B., Pope, C.A., Apte, J.S., Brauer, M., Cohen, A., Weichenthal, S., Coggins, J., Di, Q., Brunekreef, B., Frostad, J., Lim, S.S., Kan, H., Walker, K.D., Thurston, G.D., Hayes, R.B., Lim, C.C., Turner, M.C., Jerrett, M., Krewski, D., Gapstur, S.M., Diver, W.R., Ostro, B., Goldberg, D., Crouse, D.L., Martin, R.V., Peters, P., Pinault, L., Tjepkema, M., van Donkelaar, A., Villeneuve, P.J., Miller, A.B., Yin, P., Zhou, M., Wang, L., Janssen, N.A.H., Marra, M., Atkinson, R.W., Tsang, H., Quoc Thach, T., Cannon, J.B., Allen, R.T., Hart, J.E., Laden, F., Cesaroni, G., Forastiere, F., Weinmayr, G., Jaensch, A., Nagel, G., Concin, H., Spadaro, J.V., Burnett, R., Chen, H., Szyszkowicz, M., Fann, N., Hubbell, B., Pope, C.A., Apte, J.S., Brauer, M., Cohen, A., Weichenthal, S., Coggins, J., Di, Q., Brunekreef, B., Frostad, J., Lim, S.S., Kan, H., Walker, K.D., Thurston, G.D., Hayes, R.B., Lim, C.C., Turner, M.C., Jerrett, M., Krewski, D., Gapstur, S.M., Diver, W.R., Ostro, B., Goldberg, D., Crouse, D.L., Martin, R.V., Peters, P., Pinault, L., Tjepkema, M., van Donkelaar, A., Villeneuve, P.J., Miller, A.B., Yin, P., Zhou, M., Wang, L., Janssen, N.A.H., Marra, M., Atkinson, R.W., Tsang, H., Quoc Thach, T., Cannon, J.B., Allen, R.T., Hart, J.E., Laden, F., Cesaroni, G., Forastiere, F., Weinmayr, G., Jaensch, A., Nagel, G., Concin, H., Spadaro, J.V., Burnett, R., Chen, H., Szyszkowicz, M., Fann, N., Hubbell, B., Pope, C.A., Apte, J.S., Brauer, M., Cohen, A., Weichenthal, S., Coggins, J., Di, Q., Brunekreef, B., Frostad, J., Lim, S.S., Kan, H., Walker, K.D., Thurston, G.D., Hayes, R.B., Lim, C.C., Turner, M.C., Jerrett, M., Krewski, D., Gapstur, S.M., Diver, W.R., Ostro, B., Goldberg, D., Crouse, D.L., Martin, R.V., Peters, P., Pinault, L., Tjepkema, M., van Donkelaar, A., Villeneuve, P.J., Miller, A.B., Yin, P., Zhou, M., Wang, L., Janssen, N.A.H., Marra, M., Atkinson, R.W., Tsang, H., Quoc Thach, T., Cannon, J.B., Allen, R.T., Hart, J.E., Laden, F., Cesaroni, G., Forastiere, F., Weinmayr, G., Jaensch, A., Nagel, G., Concin, H., Spadaro, J.V., 2018. Global estimates of mortality associated with long-term exposure to outdoor fine particulate matter. Proc. Natl. Acad. Sci. 115, 9592–9597. https://doi.org/10.1073/pnas.1803222115

Cao, J., Situ, S., Hao, Y., Xie, S., Li, L., 2022. Enhanced summertime ozone and SOA from biogenic volatile organic compound (BVOC) emissions due to vegetation biomass variability during 1981–2018 in China. Atmospheric Chem. Phys. 22, 2351–2364. https://doi.org/10.5194/acp-22-2351-2022

Chowdhury, S., Pozzer, A., Haines, A., Klingmueller, K., Muenzel, T., Paasonen, P., Sharma, A., Venkataraman, C., Lelieveld, J., 2022. Global health burden of ambient PM2. 5 and the contribution of anthropogenic black carbon and organic aerosols. Environ. Int. 159, 107020.

Cohen, A.J., Brauer, M., Burnett, R., Anderson, H.R., Frostad, J., Estep, K., Balakrishnan, K., Brunekreef, B., Dandona, L., Dandona, R., Feigin, V., Freedman, G., Hubbell, B., Jobling, A., Kan, H., Knibbs, L., Liu, Y., Martin, R., Morawska, L., Pope, C.A., Shin, H., Straif, K., Shaddick, G., Thomas, M., van Dingenen, R., van Donkelaar, A., Vos, T., Murray, C.J.L., Forouzanfar, M.H., 2017. Estimates and 25-year trends of the global burden of disease attributable to ambient air pollution: an analysis of data from the Global Burden of Diseases Study 2015. The Lancet 389, 1907–1918. https://doi.org/10.1016/S0140-6736(17)30505-6

Emery, C., Liu, Z., Russell, A.G., Odman, M.T., Yarwood, G., Kumar, N., 2017. Recommendations on statistics and benchmarks to assess photochemical model performance. J. Air Waste Manag. Assoc. 67, 582–598. https://doi.org/10.1080/10962247.2016.1265027

Friedl, M., Sulla-Menashe, D., 2019. MCD12Q1 MODIS/Terra+Aqua Land Cover Type Yearly L3 Global 500m SIN Grid V006. https://doi.org/10.5067/MODIS/MCD12Q1.006

Fuhrer, J., Skärby, L., Ashmore, M.R., 1997. Critical levels for ozone effects on vegetation in Europe. Environ. Pollut. 97, 91–106. https://doi.org/10.1016/S0269-7491(97)00067-5

Guenther, A., Jiang, X., Shah, T., Huang, L., Kemball-Cook, S., Yarwood, G., 2020a. Model of Emissions of Gases and Aerosol from Nature Version 3 (MEGAN3) for Estimating Biogenic Emissions, in: Mensink, C., Gong, W., Hakami, A. (Eds.), Air Pollution Modeling and Its Application XXVI, Springer Proceedings in Complexity. Springer International Publishing, Cham, pp. 187–192. https://doi.org/10.1007/978-3-030-22055-6_29

Guenther, A., Jiang, X., Shah, T., Huang, L., Kemball-Cook, S., Yarwood, G., 2020b. Model of Emissions of Gases and Aerosol from Nature Version 3 (MEGAN3) for Estimating Biogenic Emissions, in: Mensink, C., Gong, W., Hakami, A. (Eds.), Air Pollution Modeling and Its Application XXVI, Springer Proceedings in Complexity. Springer International Publishing, Cham, pp. 187–192. https://doi.org/10.1007/978-3-030-22055-6_29

Guenther, A.B., Jiang, X., Heald, C.L., Sakulyanontvittaya, T., Duhl, T., Emmons, L.K., Wang, X., 2012a. The Model of Emissions of Gases and Aerosols from Nature version 2.1 (MEGAN2.1): an extended and updated framework for modeling biogenic emissions. Geosci. Model Dev. 5, 1471–1492. https://doi.org/10.5194/gmd-5-1471-2012

Guenther, A.B., Jiang, X., Heald, C.L., Sakulyanontvittaya, T., Duhl, T., Emmons, L.K., Wang, X., 2012b. The Model of Emissions of Gases and Aerosols from Nature version 2.1 (MEGAN2.1): an extended and updated framework for modeling biogenic emissions. Geosci. Model Dev. 5, 1471–1492. https://doi.org/10.5194/gmd-5-1471-2012

He, C.Q., Zou, Y., Lv, S.J., Flores, R.M., Yan, X.L., Deng, T., Deng, X.J., 2024. The importance of photochemical loss to source analysis and ozone formation potential: Implications from in-situ observations of volatile organic compounds (VOCs) in Guangzhou, China. Atmos. Environ. 320, 120320. https://doi.org/10.1016/j.atmosenv.2023.120320

Le Page, Y., Morton, D., Bond-Lamberty, B., Pereira, J.M.C., Hurtt, G., 2015. HESFIRE: a global fire model to explore the role of anthropogenic and weather drivers. Biogeosciences 12, 887–903. https://doi.org/10.5194/bg-12-887-2015

Lelieveld, J., Klingmüller, K., Pozzer, A., Burnett, R.T., Haines, A., Ramanathan, V., 2019. Effects of fossil fuel and total anthropogenic emission removal on public health and climate. Proc. Natl. Acad. Sci. 116, 7192–7197. https://doi.org/10.1073/pnas.1819989116

Lelieveld, J., Pozzer, A., Pöschl, U., Fnais, M., Haines, A., Münzel, T., 2020. Loss of life expectancy from air pollution compared to other risk factors: a worldwide perspective. Cardiovasc. Res. 116, 1910–1917.

Lohmann, U., Rotstayn, L., Storelvmo, T., Jones, A., Menon, S., Quaas, J., Ekman, A.M.L., Koch, D., Ruedy, R., 2010. Total aerosol effect: radiative forcing or radiative flux perturbation? Atmospheric Chem. Phys. 10, 3235–3246. https://doi.org/10.5194/acp-10-3235-2010

Lombardozzi, D., Levis, S., Bonan, G., Hess, P.G., Sparks, J.P., 2014. The Influence of Chronic Ozone Exposure on Global Carbon and Water Cycles. J. Clim. 28, 292–305. https://doi.org/10.1175/JCLI-D-14-00223.1

Lu, X., Zhang, L., Wang, X., Gao, M., Li, K., Zhang, Yuzhong, Yue, X., Zhang, Yuanhang, 2020. Rapid Increases in Warm-Season Surface Ozone and Resulting Health Impact in China Since 2013. Environ. Sci. Technol. Lett. 7, 240–247. https://doi.org/10.1021/acs.estlett.0c00171

Luecken, D.J., Yarwood, G., Hutzell, W.T., 2019. Multipollutant modeling of ozone, reactive nitrogen and HAPs across the continental US with CMAQ-CB6. Atmos. Environ. 201, 62–72. https://doi.org/10.1016/j.atmosenv.2018.11.060

Ma, H., Liang, S., 2022. Development of the GLASS 250-m leaf area index product (version 6) from MODIS data using the bidirectional LSTM deep learning model. Remote Sens. Environ. 273, 112985. https://doi.org/10.1016/j.rse.2022.112985

Ma, M., Gao, Y., Ding, A., Su, H., Liao, H., Wang, S., Wang, X., Zhao, B., Zhang, S., Fu, P., Guenther, A.B., Wang, M., Li, S., Chu, B., Yao, X., Gao, H., 2022. Development and Assessment of a High-Resolution Biogenic Emission Inventory from Urban Green Spaces in China. Environ. Sci. Technol. 56, 175–184. https://doi.org/10.1021/acs.est.1c06170

Ma, M., Gao, Y., Wang, Y., Zhang, S., Leung, L.R., Liu, C., Wang, S., Zhao, B., Chang, X., Su, H., Zhang, T., Sheng, L., Yao, X., Gao, H., 2019. Substantial ozone enhancement over the North China Plain from increased biogenic emissions due to heat waves and land cover in summer 2017. Atmospheric Chem. Phys. 19, 12195–12207.

https://doi.org/10.5194/egusphere-2024-1163
Preprint. Discussion started: 25 June 2024

https://doi.org/10.5194/acp-19-12195-2019

Masson-Delmotte, V., Zhai, P., Pirani, A., Connors, S.L., Péan, C., Berger, S., Caud, N., Chen, Y., Goldfarb, L., Gomis, M., others, 2021. Climate change 2021: the physical science basis. Contrib. Work. Group Sixth Assess. Rep. Intergov. Panel Clim. Change 2.

Meng, Y., Song, J., Zeng, L., Zhang, Y., Zhao, Y., Liu, X., Guo, H., Zhong, L., Ou, Y., Zhou, Y., Zhang, T., Yue, D., Lai, S., 2022. Ambient volatile organic compounds at a receptor site in the Pearl River Delta region: Variations, source apportionment and effects on ozone formation. J. Environ. Sci. 111, 104–117. https://doi.org/10.1016/j.jes.2021.02.024

Myneni, R., Knyazikhin, Y., Park, T., 2015. MOD15A2H MODIS/Terra leaf area Index/FPAR 8-Day L4 global 500m SIN grid V006. NASA EOSDIS Land Process. DAAC.

National Centers for Environmental Prediction, National Weather Service, NOAA, U.S. Department of Commerce, 2000. NCEP FNL Operational Model Global Tropospheric Analyses, continuing from July 1999.

Pye, H.O.T., Murphy, B.N., Xu, L., Ng, N.L., Carlton, A.G., Guo, H., Weber, R., Vasilakos, P., Appel, K.W., Budisulistiorini, S.H., Surratt, J.D., Nenes, A., Hu, W., Jimenez, J.L., Isaacman-VanWertz, G., Misztal, P.K., Goldstein, A.H., 2017. On the implications of aerosol liquid water and phase separation for organic aerosol mass. Atmospheric Chem. Phys. 17, 343–369. https://doi.org/10.5194/acp-17-343-2017

Qiu, J., Fang, C., Tian, N., Wang, H., Wang, J., 2023. Impacts of land use and land cover changes on local meteorology and PM2.5 concentrations in Changchun, Northeast China. Atmospheric Res. 289, 106759. https://doi.org/10.1016/j.atmosres.2023.106759

Ramanathan, V., Chung, C., Kim, D., Bettge, T., Buja, L., Kiehl, J.T., Washington, W.M., Fu, Q., Sikka, D.R., Wild, M., 2005. Atmospheric brown clouds: Impacts on South Asian climate and hydrological cycle. Proc. Natl. Acad. Sci. 102, 5326–5333. https://doi.org/10.1073/pnas.0500656102

Ramanathan, V., Crutzen, P.J., Kiehl, J.T., Rosenfeld, D., Ramanathan, V., Crutzen, P.J., Kiehl, J.T., Rosenfeld, D., Ramanathan, V., Crutzen, P.J., Kiehl, J.T., Rosenfeld, D., 2001. Aerosols, Climate, and the Hydrological Cycle. Science 294, 2119–2124. https://doi.org/10.1126/science.1064034

Salamanca, F., Martilli, A., Tewari, M., Chen, F., 2011. A Study of the Urban Boundary Layer Using Different Urban Parameterizations and High-Resolution Urban Canopy Parameters with WRF. J. Appl. Meteorol. Climatol. 50, 1107–1128. https://doi.org/10.1175/2010JAMC2538.1

Schlaerth, H.L., Silva, S.J., Li, Y., 2023. Characterizing Ozone Sensitivity to Urban Greening in Los Angeles Under Current Day and Future Anthropogenic Emissions Scenarios. J. Geophys. Res. Atmospheres 128, e2023JD039199. https://doi.org/10.1029/2023JD039199

Seinfeld, J.H., Pandis, S.N., Noone, K., 1998. *Atmospheric Chemistry and Physics: From Air Pollution to Climate Change.* Phys. Today 51, 88–90. https://doi.org/10.1063/1.882420

Shan, D., Du, Z., Zhang, T., Zhang, X., Cao, G., Liu, Z., Yao, Z., Tang, K., Liang, S., 2023. Variations, sources, and effects on ozone formation of VOCs during ozone episodes in 13 cities in China. Front. Environ. Sci. 10, 1084592. https://doi.org/10.3389/fenvs.2022.1084592

Shindell, D., Kuylenstierna, J.C.I., Vignati, E., van Dingenen, R., Amann, M., Klimont, Z., Anenberg, S.C., Muller, N., Janssens-Maenhout, G., Raes, F., Schwartz, J., Faluvegi, G., Pozzoli, L., Kupiainen, K., Höglund-Isaksson, L., Emberson, L., Streets, D., Ramanathan, V., Hicks, K., Oanh, N.T.K., Milly, G., Williams, M., Demkine, V., Fowler, D., Shindell, D., Kuylenstierna, J.C.I., Vignati, E., van Dingenen, R., Amann, M., Klimont, Z., Anenberg, S.C., Muller, N., Janssens-Maenhout, G., Raes, F., Schwartz, J., Faluvegi, G., Pozzoli, L., Kupiainen, K., Höglund-Isaksson, L., Emberson, L., Streets, D., Ramanathan, V., Hicks, K., Oanh, N.T.K., Milly, G., Williams, M., Demkine, V., Fowler, D., Shindell, D., Kuylenstierna, J.C.I., Vignati, E., van Dingenen, R., Amann, M., Klimont, Z., Anenberg, S.C., Muller, N., Janssens-Maenhout, G., Raes, F., Schwartz, J., Faluvegi, G., Pozzoli, L., Kupiainen, K., Höglund-Isaksson, L., Emberson, L., Streets, D., Ramanathan, V., Hicks, K., Oanh, N.T.K., Milly, G., Williams, M., Demkine, V., Fowler, D., 2012. Simultaneously Mitigating Near-Term Climate Change and Improving Human Health and Food Security. Science 335, 183–189. https://doi.org/10.1126/science.1210026

Sindelarova, K., Granier, C., Bouarar, I., Guenther, A., Tilmes, S., Stavrakou, T., Müller, J.-F., Kuhn, U., Stefani, P., Knorr, W., 2014. Global data set of biogenic VOC emissions calculated by the MEGAN model over the last 30 years. Atmospheric Chem. Phys. 14, 9317–9341. https://doi.org/10.5194/acp-14-9317-2014

Soleimanian, E., Wang, Y., Li, W., Liu, X., Griggs, T., Flynn, J., Walter, P.J., Estes, M.J., 2023. Understanding ozone episodes during the TRACER-AQ campaign in Houston, Texas: The role of transport and ozone production sensitivity to precursors. Sci. Total Environ. 900, 165881. https://doi.org/10.1016/j.scitotenv.2023.165881

Solomon, S., 2007. Climate change 2007-the physical science basis: Working group I contribution to the fourth assessment report of the IPCC. Cambridge university press.

Wang, H., Liu, Z., Wu, K., Qiu, J., Zhang, Y., Ye, B., He, M., 2022. Impact of Urbanization on Meteorology and Air Quality in Chengdu, a Basin City of Southwestern China. Front. Ecol. Evol. 10, 845801. https://doi.org/10.3389/fevo.2022.845801

Wang, H., Liu, Z., Zhang, Y., Yu, Z., Chen, C., 2021. Impact of different urban canopy models on air quality simulation in Chengdu, southwestern China. Atmos. Environ. 267, 118775. https://doi.org/10.1016/j.atmosenv.2021.118775

Wang, P., Chen, Y., Hu, J., Zhang, H., Ying, Q., 2019. Attribution of Tropospheric Ozone to NO_x and VOC Emissions: Considering Ozone Formation in the Transition Regime. Environ. Sci. Technol. 53, 1404–1412. https://doi.org/10.1021/acs.est.8b05981

WHO, 2021. WHO global air quality guidelines: particulate matter (PM2. 5 and PM10), ozone, nitrogen dioxide, sulfur dioxide and carbon monoxide. World Health Organization.

Wu, K., Yang, X., Chen, D., Gu, S., Lu, Y., Jiang, Q., Wang, K., Ou, Y., Qian, Y., Shao, P., Lu, S., 2020. Estimation of biogenic VOC emissions and their corresponding impact on ozone and secondary organic aerosol formation in China. Atmospheric Res. 231, 104656. https://doi.org/10.1016/j.atmosres.2019.104656

Yao, Z., Huang, G., 2023. Effects of Land Use Changes Across Different Urbanization Periods on Summer Rainfall in the Pearl River Delta Core Area. Int. J. Disaster Risk Sci. 14, 458–474. https://doi.org/10.1007/s13753-023-00497-8

Yim, S.H.L., Wang, M., Gu, Y., Yang, Y., Dong, G., Li, Q., 2019. Effect of Urbanization on Ozone and Resultant Health Effects in the Pearl River Delta Region of China. J. Geophys. Res. Atmospheres 124, 11568–11579. https://doi.org/10.1029/2019JD030562

Zhao, Y., Xi, M., Zhang, Q., Dong, Z., Ma, M., Zhou, K., Xu, W., Xing, J., Zheng, B., Wen, Z., Liu, X., Nielsen, C.P., Liu, Y., Pan, Y., Zhang, L., 2022. Decline in bulk deposition of air pollutants in China lags behind reductions in emissions. Nat. Geosci. 15, 190–195. https://doi.org/10.1038/s41561-022-00899-1

Zheng, J., Shao, M., Che, W., Zhang, L., Zhong, L., Zhang, Y., Streets, D., 2009. Speciated VOC Emission Inventory and Spatial Patterns of Ozone Formation Potential in the Pearl River Delta, China. Environ. Sci. Technol. 43, 8580–8586. https://doi.org/10.1021/es901688e

Zhou, D., Zhao, S., Zhang, L., Sun, G., Liu, Y., 2015. The footprint of urban heat island effect in China. Sci. Rep. 5, 11160.